Third ARO Workshop on Smart Structures

Sponsored by:

U.S. Army Research Office
Research Triangle Park, North Carolina

Hosted by:

Center for Intelligent Material Systems and Structures
Virginia Polytechnic Institute and State University

Virginia Tech

August 27–29, 1997

Donaldson Brown Hotel and Conference Center ■ Blacksburg, Virginia

WIND TUNNEL TESTING OF A SMALL-SCALE ROTOR WITH ON-BLADE ELEVONS

Mark V. Fulton
Aeromechanics Branch
Army/NASA Rotorcraft Division

and

Robert A. Ormiston
Aeroflightdynamics Directorate
US Army Aviation RD&E Center (AMCOM)

Ames Research Center
Moffett Field, California

Introduction

There has long been a desire to reduce helicopter vibration. Considerable effort is now being directed toward on-blade aerodynamic control concepts. The present investigation uses a trailing-edge control surface, or elevon, to generate local aerodynamic lift and pitching moment.

In the present investigation a two-blade, 7.5-ft diameter hingeless rotor with 10% chord on-blade elevons driven by piezoceramic bimorph actuators was tested in forward flight for advance ratios from 0.1 to 0.3 at low to moderate thrust coefficients. The objective was to explore fundamental dynamic response characteristics and determine the effectiveness of elevon control in reducing blade vibratory loads. All elevon excitations were open loop. Primary measurements included elevon deflection and blade root bending and torsion moments. The design and development of the model rotor blades, piezoceramic actuators and elevons, and quasi-steady and dynamic test data for nonrotating and rotating conditions in hover were reported in Ref. 1. Preliminary results of forward flight wind tunnel testing will be presented herein.

Experimental Model

A low tip-speed (298 ft/sec), small-scale dynamic model of low cost and complexity was suitable for this exploratory investigation. Fundamental structural dynamic characteristics were emphasized; evaluation of rotor performance and compressibility or stall effects would require a more sophisticated model. The model is shown in Fig. 1 installed on the Small Scale Rotor Test Rig (RTR) in the Army/NASA 7-by 10-Ft. Wind Tunnel.

The 7.5-ft diameter rectangular, untwisted rotor blades are uniform in mass and stiffness except at the blade root and the elevon "active section". Chordwise mass and aerodynamic centers are located near the quarter chord of the symmetrical NACA 0012 airfoil section. The blades are constructed of composite materials including a fiberglass spar, foam filled core, and fiberglass wrapped skin construction. Each blade has two bimorph actuators driving a single, 10% chord, plain elevon with a span of 12% blade radius, centered at the 75% radial location. Model physical properties and operating conditions are listed in Table 1. Additional construction details are available in Ref. 1.

The two piezoceramic, lead zirconate titanate (PZT), bimorph bender beam actuators are cantilevered to the rear of each blade spar. Fiberglass lever arms project forward from the elevon to engage the tip of the cantilever PZT beam to produce elevon rotational motion. In order to minimize mechanical losses, considerable attention was devoted to the design and construction of the elevon hinge and lever mechanism. To reduce friction, steel pins bonded to the ends of the PZT bender beams engaged the elevon lever arms. Slots in the lever arms accommodated small translations of the bender beam pins caused by the opposing arc motion of the two components, Fig. 2. Steel elevon hinge pins were mounted in low friction Delrin bearing blocks attached to the blade, with brass and Teflon thrust washers reacting the elevon centrifugal force. A photograph of the actuator and elevon installation is shown in Fig. 3.

Elevon motion was measured with a Hall-effect transducer and blade moment responses were measured through full strain gage bridges at the root flexure of each blade. The flap and chord strain gage bridges were at 0.114 R, and the torsion strain gage

Presented at the Third ARO Workshop on Smart Structures, Virginia Tech, Blacksburg, VA, August 27-29, 1997.

bridge was at 0.128 R. In addition, the root pitch of blade 1 was measured with a potentiometer.

Rotor Blade Structural Dynamic Characteristics

The rotor blade frequency fan plot (in air at 0° collective pitch), Fig. 4, illustrates the structural dynamic characteristics of the rotor blades. The frequencies were predicted by Second Generation Comprehensive Helicopter Analysis System (2GCHAS) using blade properties adjusted to match measured nonrotating frequencies. The nominal rotor speed (760 RPM, 12.7 Hz) results in a representative first-flap frequency (1.11/rev). The rotor is stiff inplane, with a first lead-lag frequency of 1.08/rev, and was somewhat sensitive to 1/rev loads. The second flap bending mode is above 3/rev unlike most blades, where this mode is below 3/rev. The first torsion frequency is 4.6/rev. Both the first elevon/actuator and third flap bending frequencies are between 6/rev and 7/rev at nominal rotor speed. The bimorph/elevon fundamental natural frequency was estimated assuming quasi-static 2-D airfoil aerodynamics and ignoring mechanical friction.

Synopsis of Previous Hover Test Data

The hover testing was conducted in the AFDD Hover Test Chamber on the RTR. The principal results of the hover testing are summarized in this section. Additional details can be found in Ref. 1.

The model succeeded in demonstrating the practical feasibility of using piezoceramic bimorph actuators to provide reasonable elevon deflections for a small-scale low tip speed model by achieving deflections of +/- 10 deg nonrotating and +/- 5 deg up to 4/rev at the nominal rotor speed of 760 RPM.

Low-frequency blade torsion moment response to elevon deflection indicated that elevon effectiveness was lower than predicted by thin airfoil theory, largely due to the effects of low Reynolds number on elevon control power, $c_{m\delta}$.

Low frequency blade root bending response exhibited an "elevon reversal speed" slightly above 760 RPM, due to elastic blade twist induced by the negative elevon aerodynamic pitching moment.

Aeroelastic and structural dynamic response characteristics were evaluated over a wide rotor speed range using sine sweep excitation of the elevon up to 105 Hz (8/rev). CIFER® (Refs. 2 and 3) was used to calculate the frequency response function magnitude, phase and coherence of measured blade flap bending and torsion moments to elevon input and elevon response to actuator input voltage.

Frequency response measurements indicated that blade torsion moment response at resonance was amplified approximately five times the steady-state amplitude.

Blade flap bending responses produced by the available range of elevon deflection suggested that it would be possible to achieve significant reductions of anticipated 3, 4, and 5/rev vibratory flap bending moments in forward flight.

Wind Tunnel Test Procedures

Forward flight testing was conducted in the Army/NASA 7-by 10-Ft. Wind Tunnel. Testing was typically performed at 760 and 450 RPM, with 760 being the "nominal" rotor speed, although limited testing was also performed at 600 RPM. Most of the data was taken at zero deg shaft angle, although a few points were also taken with 3 deg forward shaft tilt.

Steady-state data was obtained to quantify the variation of the root blade vibratory loads with flight speed. The steady-state test envelope is shown in Fig. 5 for both 760 and 450 RPM at 0 deg shaft angle and a range of advance ratios from 0 to 0.3. Since at 760 RPM the maximum achievable collective pitch was lower than desired and constrained by allowable blade loads, testing at 450 RPM was performed to obtain higher nondimensional blade loading. Figure 6 illustrates the theoretical nondimensional blade loading (thrust coefficient/solidity) reached during testing as predicted using 2GCHAS.

In addition to the steady-state testing, phase sweeps of elevon excitation were performed. First, a flight condition was established, including shaft angle, rotor speed, advance ratio, and collective pitch, with cyclic pitch adjusted to minimize 1/rev flap bending. Next, a discrete harmonic of the rotor speed (from 1/rev to 5/rev) was chosen for PZT actuator voltage excitation. A phase sweep of the PZT voltage was then performed, acquiring a data point for each discrete elevon phase angle (at the same cyclic pitch). The collective pitch used for each voltage harmonic and advance ratio is given in Table 2 for 760 RPM. For 450 RPM, all phase sweeps were at an advance ratio of 0.2 for a collective of 6.25 deg. This phase sweep data provides a measurement of elevon effectiveness and identifies the elevon phase required to minimize flap bending moment.

For a few flight conditions and elevon frequencies, a voltage sweep was performed. For these cases, a phase would be selected and the PZT voltage would be swept, with a data point being acquired for each discrete voltage level. This provides evidence of the elevon amplitude required for minimization of a flap bending harmonic.

Finally, frequency response data was acquired using frequency sweeps from 1 to 105 Hz. These frequency sweeps were performed for a range of advance ratios (up to μ = 0.6) at 0 deg collective, although some sweeps were also performed at higher collective pitch angles. It is hoped that this data will indicate any influence of advance ratio on elevon effectiveness in changing the blade root flap bending and torsion moments.

Wind Tunnel Data

Data presented in this paper is limited to 760 RPM, 0 deg shaft angle, 4 deg collective pitch, and an advance ratio of 0.2.

The basic concept of vibratory loads reduction is that aerodynamic induced blade loads generated at one elevon harmonic will cancel the steady-state periodic load at the same frequency if the amplitude and phase of the elevon excitation is properly adjusted. This assumes, of course, that the elevon has sufficient effectiveness to cancel the steady-state blade root bending. If periodic motion is assumed, with the fundamental period equal to one rotor revolution, then the steady-state moment can be represented as

$$Ms = Ms_o + \sum_{i=1}^{n} Ms_i * Cos(i\psi + \phi_{Msi}) \qquad (1)$$

where Ms_o is the steady term and Ms_i is the amplitude of the i^{th} harmonic. The same form can be used for the elevon-induced moment, Mδ, and the total resultant moment, Mt. If the rotor is assumed to respond linearly, then

$$Mt = Ms + M\delta \qquad (2)$$

In this case, the total vibratory load response can be shown to be a function of the steady-state and elevon-induced response :

$$Mt_n = \sqrt{Ms_n^2 + 2 * Ms_n * M\delta_n * Cos(\phi_{Msn} - \phi_{M\delta n}) + M\delta_n^2} \qquad (3)$$

This linear model is illustrated in Fig. 7, where the amplitude of the total response (Mt_n) is plotted as a function of the phase of the elevon-induced moment ($\phi_{M\delta n}$) for various amplitudes of the elevon-induced moment ($M\delta_n$). This figure illustrates two principal effects. First, both "underdriven" and "overdriven" conditions are shown, where the excitation input is either insufficient or excessive for countering the steady-state response, respectively. Second, cancellation is shown to require 180 deg phasing of the elevon-induced moment relative to the steady-state moment.

Several results for the phase sweeps are now described. For each case, the amplitude of the response is obtained using an FFT of the response at the excitation harmonic. In each case, the amplitudes for blade "j" are plotted against the phase of elevon "j" (relative to blade "j" aft, for "j" = 1 or 2). The 5/rev elevon deflection amplitude, Fig. 8, shows that there is only a small variation of the elevon amplitude with elevon phase.

The resultant variation in the 5/rev flap bending moment, however, is significant (Fig. 9). Note that the two blades show significantly different steady-state response, but that they also both show significant sensitivity to elevon phase angle. Similar flap bending results are shown in Figs. 10 and 11 for 4/rev and 3/rev excitation, respectively. Note, however, that the 3/rev elevon motion is of the proper magnitude to provide nearly complete cancellation of the 3/rev flap bending moment for a phase of about 90 deg (Fig. 11).

Figures 9 - 11 include curve fits based on the linear model of Eq. 3, with the magnitude of the steady-state harmonic specified but the remaining variables left as free parameters. This approach provides good curve fits and permits the identification of the amplitude and phase of the elevon-induced moment. Both the steady-state harmonic and the elevon-induced harmonic are plotted for 1/rev - 5/rev in Fig. 12. (Each amplitude is at the frequency of the PZT voltage.) Comparing the relative amplitudes of these two components provides an indication of elevon effectiveness for each response harmonic. The results in Fig. 12 indicate that, at this flight condition (μ = 0.2 and θ_o = 4 deg), elevon effectiveness is sufficient to cancel the flap bending moment at all harmonics except 2/rev. Although the test data was obtained at different voltage levels, this comparison is useful since only the 1/rev and 2/rev voltage levels were at the maximum allowable value of 110 Vrms.

The measured flap bending moment response characteristics derived from the curve fits will now be used to illustrate how vibratory loads vary as a function of elevon excitation amplitude. The average

elevon amplitude (δ_n) at the PZT excitation frequency of each harmonic shown in Fig. 12 can be used to normalize the results. First, assume that the elevon-induced moment is proportional to elevon angle. Next, assume that the phase of the elevon motion is chosen to minimize the total response. The steady-state response at each harmonic can then be used with the elevon effectiveness at each harmonic to predict the variation of the total response at any given harmonic with elevon angle:

$$Mt_n = \left| Ms_n - \left(\frac{M\delta_n}{\delta_n} \right) * \delta \right| \qquad (4)$$

The results of using this procedure are shown in Fig. 13 where the flap bending moment is reduced for increasing elevon deflection amplitude until cancellation is achieved; for larger elevon motions, an "overdriven" condition begins, causing the total response to increase.

The azimuthal time history shown in Fig. 14 illustrates several features of the elevon motion response. Consider two data points corresponding to the 4/rev harmonic line in Fig. 13: first the steady-state response and, second, the point with the 4P elevon excitation amplitude chosen to cancel the 4P flap bending harmonic. The elevon motion shown in Fig. 14 for the steady-state case is very small, as would be expected. The large 4/rev elevon motion required to cancel the 4/rev flap bending moment exhibits moderate 1/rev content as well as other harmonics. This is due in part to the azimuthal variation of elevon aerodynamic "stiffness" opposing the PZT actuator deflection; these nonsinusoidal elevon motions may complicate future correlations with analytical predictions.

Nonetheless, the desired effect of significantly reducing the 4/rev flap bending moment was accomplished as shown in Fig. 15. The fact that harmonics other than 4/rev are affected is likely caused by interharmonic coupling induced by the periodic coefficients of forward flight. Likewise, the nonsinusoidal elevon motion may well be affected by the blade motion through aerodynamic and inertial effects. Further detailed data analysis and correlation with analytical predictions will be required to better determine the exact cause of the observed behaviors.

Concluding Remarks

Preliminary examination of the experimental data from this wind tunnel test indicates the on-blade elevon concept may have significant potential for reducing rotor system vibratory loads. Further evaluation of the data together with analytical studies are planned. A complete evaluation of the practical effectiveness and suitability of active on-blade elevon controls will require additional testing with more sophisticated rotor models.

References

1. Fulton, M.V., and Ormiston, R.A., "Hover Testing of a Small-Scale Rotor with On-Blade Elevons," *Proceedings of the 53rd Annual Forum of the American Helicopter Society*, Virginia Beach, Virginia, April 29-May 1, 1997.

2. Tischler, M.B., Cauffman, M.G., "Frequency-Response Method for Rotorcraft System Identification: Flight Applications to BO-105 Coupled Rotor/Fuselage Dynamics," *Journal of the American Helicopter Society*, Vol. 37, No. 3, July 1992, pp. 3-17.

3. Tischler, M.B., Driscoll, J.T., Cauffman, M.G., and Freedman, C.J., "Study of Bearingless Main Rotor Dynamics from Frequency-Response Wind Tunnel Test Data," *Presented at the American Helicopter Conference*, San Francisco, CA, January 19-21, 1994.

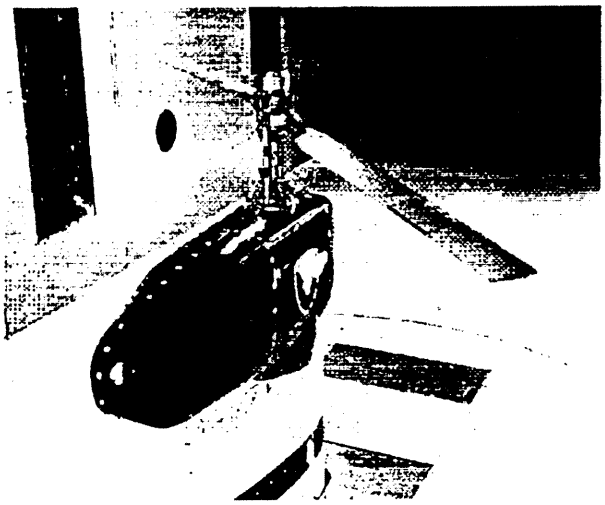

Fig. 1 Rotor with on-blade elevons in the Army/NASA 7- by 10-Ft. Wind Tunnel.

Table 1. Rotor Characteristics & Operating Conditions.

Description	Variable	Value
No. of Blades	b	2
Rotor Radius	R	45 in (3.75 ft)
Airfoil		NACA 0012
Airfoil Chord	c	3.4 in
Elevon Chord	c_{elv}	0.34 in (10% c)
Elevon Span	S_{elv}	5.55 in (12% R)
Solidity	σ	0.048
Lock No.	γ	5 -- 7.5
Precone	β_0	0.0
Nominal Rotor Speed	Ω_0	760 RPM (12.7 Hz)
1st Flap Mode	$\omega_{\beta 1}$	1.11/rev*
1st Lag Mode	$\omega_{\zeta 1}$	1.08/rev*
1st Torsion Mode	$\omega_{\phi 1}$	4.6/rev*
Airspeed	V_{tip}, V_{elv}	298, 224 ft/s
Dynamic Pressure	q_{tip}, q_{elv}	106, 60 lb/ft^2
Reynolds Number	Re_{tip}, Re_{elv}	540,000; 400,000
Mach Number	M_{tip}, M_{elv}	0.27, 0.20

* θ_0=0°, 760 RPM, in air

Table 2. Collective pitch angles for elevon phase sweep test matrix at 760 RPM (0 deg shaft angle).

ω/μ	0.1	0.2	0.3
1		0°, 2°, 3°, 4°	
2		0°, 2°, 3°, 4°	
3	2°	0°, 2°, 3°, 4°	2°
4	2°, 3°	0°, 2°, 3°, 4°	2°, 3°
5	2°	0°, 2°, 3°, 4°	2°

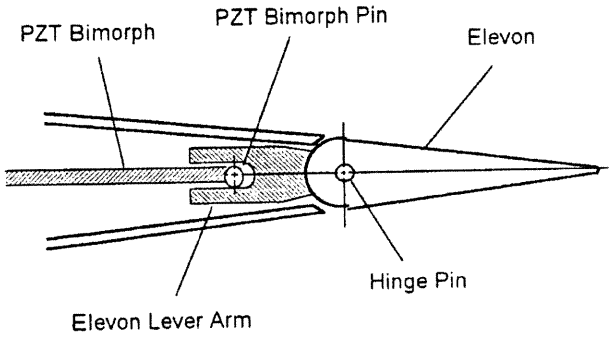

Fig. 2 Airfoil cross section, PZT bimorph bender beam and elevon lever arm mechanism.

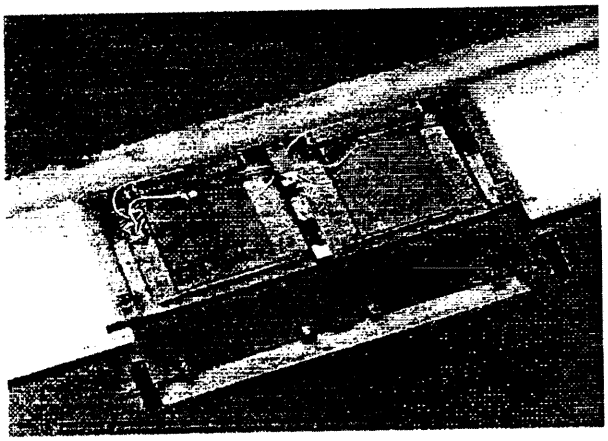

Fig. 3 Close-up of the active section with the access panel removed and the elevon disassembled.

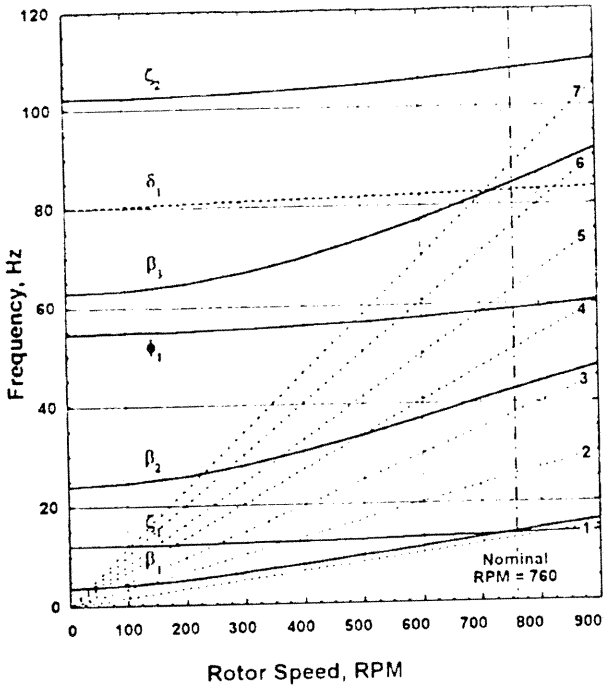

Fig. 4 Rotor blade frequencies versus rotor speed in air at zero collective pitch.

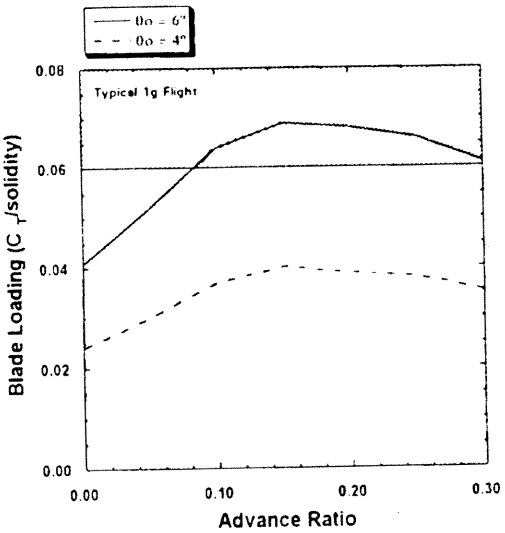

Fig. 6 Representative blade loading (760 RPM).

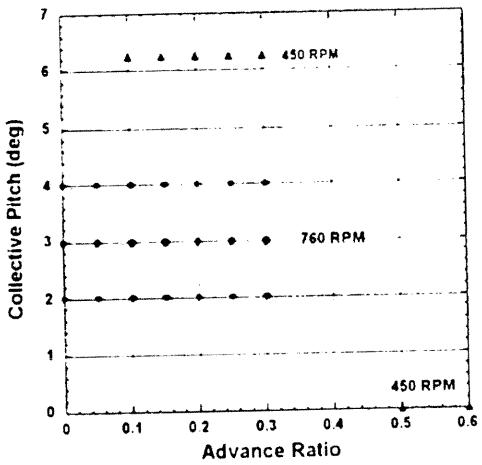

Fig. 5 Steady-state test matrix (760 and 450 RPM at 0 deg shaft angle).

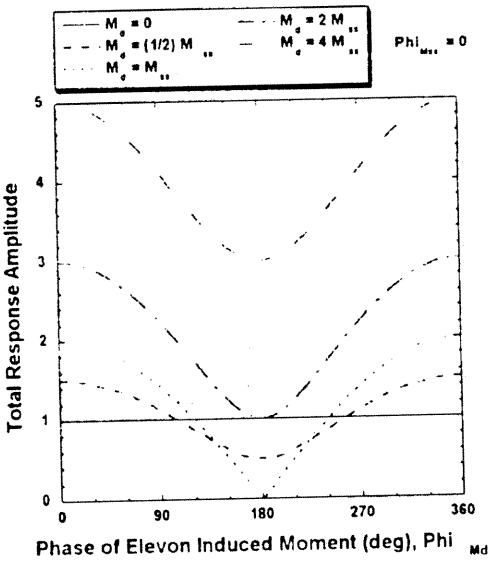

Fig. 7 Linear model of sine wave summation.

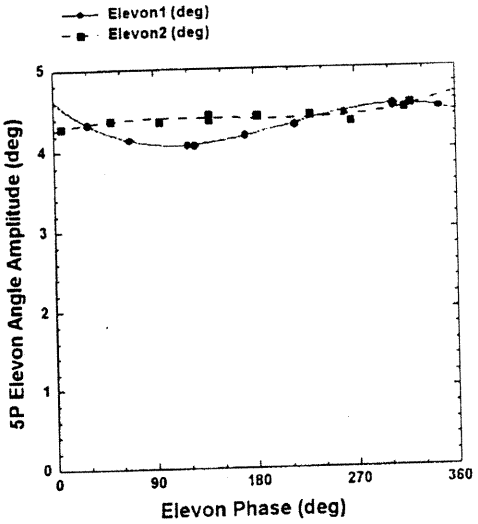

Fig. 8 Relative insensitivity of 5/rev elevon motion to elevon phase (5/rev PZT voltage).

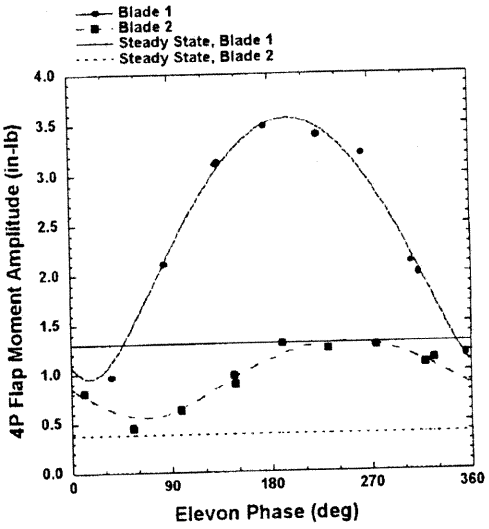

Fig. 10 Sensitivity of 4/rev flap bending moment to elevon phase (4/rev PZT voltage).

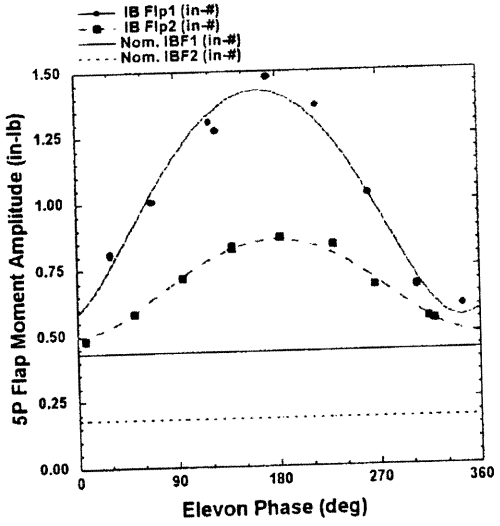

Fig. 9 Sensitivity of 5/rev flap bending moment to elevon phase (5/rev PZT voltage).

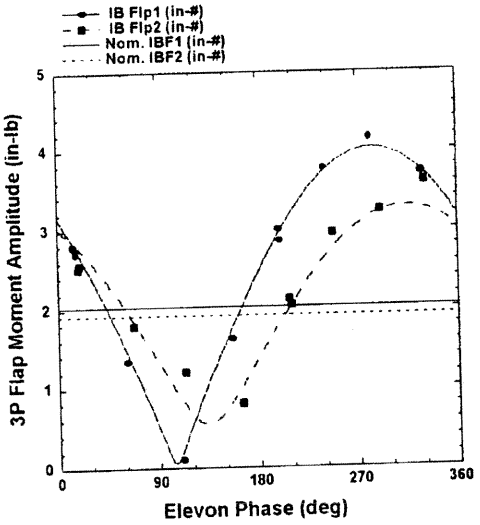

Fig. 11 Sensitivity of 3/rev flap bending moment to elevon phase (3/rev PZT voltage).

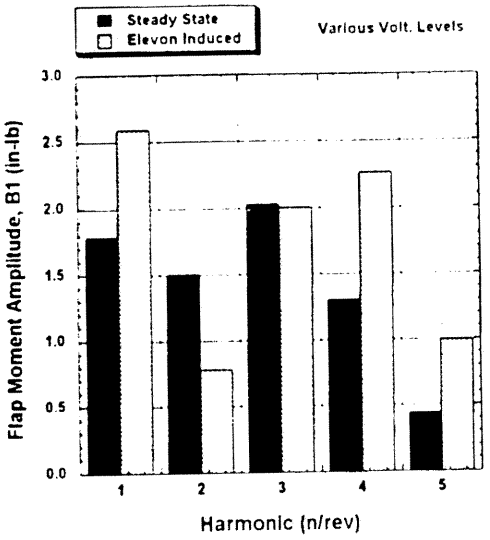

Fig. 12 Elevon effectiveness for various harmonics.

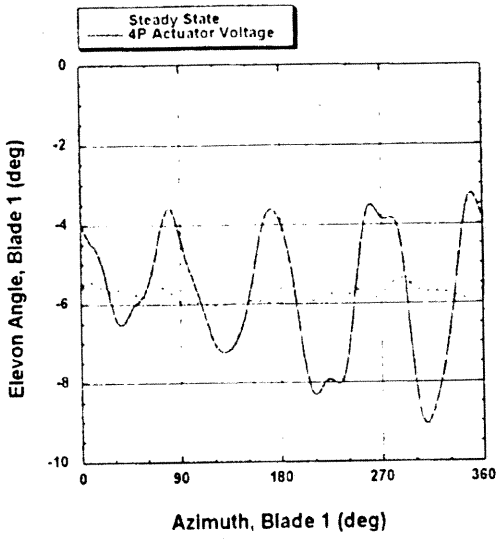

Fig. 14 Elevon motion over one rotor revolution for two cases, one with 4/rev PZT voltage and the other without.

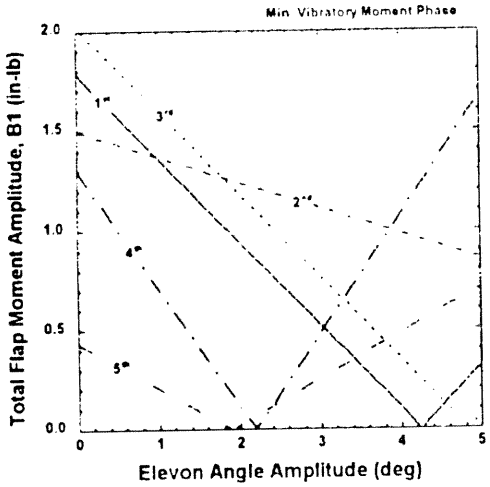

Fig. 13 Effect of elevon excitation amplitude on flap bending moment harmonics; derived from experimental measurements.

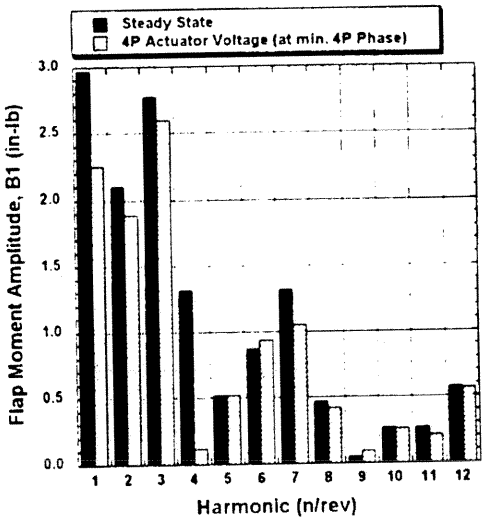

Fig. 15 Comparison of flap bending moment amplitudes for steady-state condition and case with 4/rev PZT voltage.